J. Membrane Biol. 180, 49–64 (2001)
DOI: 10.1007/s002320010058

The Journal of
Membrane
Biology



# Regulation of an Outwardly Rectifying Chloride Conductance in Renal Epithelial Cells by External and Internal Calcium

**G.S. Stewart, M. Glanville, O. Aziz, N.L. Simmons, M.A. Gray**
Department of Physiological Sciences, University Medical School, Framlington Place, Newcastle upon Tyne, NE2 4HH, UK

Received: 17 July 2000/Revised: 30 November 2000

**Abstract.** We have used perforated patch clamp and Fura-2 microfluorescence measurements to study $Ca^{2+}$-activated $Cl^-$ currents in cultured mouse renal inner medullary collecting duct cells (mIMCD-3). The conductance was spontaneously active under resting conditions and whole cell currents were time and voltage-independent with an outwardly rectifying current-voltage relationship. The channel blockers DIDS, niflumic acid, glybenclamide and NPPB reversibly decreased the basal currents, whereas the sulfhydryl agent, DTT produced an irreversible inhibition. Increasing or decreasing extracellular calcium produced parallel changes in the size of the basal currents. Variations in external $Ca^{2+}$ were associated with corresponding changes in free cytosolic $Ca^{2+}$ concentration. Increasing cytosolic $Ca^{2+}$ by extracellular ATP or ionomycin, further enhanced $Cl^-$ conductance, with whole cell currents displaying identical biophysical properties to the basal currents. However, the agonist-stimulated currents were now increased by DTT exposure, but still inhibited by the other channel blockers. Using RT-PCR, three distinct mRNA transcripts belonging to the CLCA family of $Ca^{2+}$-activated $Cl^-$ channel proteins were identified, two of which represent novel sequences. Whether different channels underlie the basal and agonist-stimulated currents in mIMCD-3 cells is unclear. Our findings establish a novel link between alterations in external and internal $Ca^{2+}$ and the activity of $Ca^{2+}$-activated $Cl^-$ transport in these cells.

**Key words:** Renal epithelial cells — Chloride channels — Intracellular calcium — Anion secretion — Patch clamp

*Correspondence to:* M.A. Gray

## Introduction

There is increasing evidence for a significant transcellular transport of $Cl^-$ and other anions by renal tubular epithelia that is mediated, in part, by regulated $Cl^-$ channels (Simmons, 1993; Husted et al., 1995). Importantly, mutations in certain $Cl^-$ channels of the ClC family result in significant renal disease (Jentsch, Friedrich & Yamada, 1999). For example, mutations in ClC-5 lead to renal stone formation (nephrolithiasis, Lloyd et al., 1996) and mutations in ClC-Kb give rise to Bartter's syndrome (Simon et al., 1997). The cystic fibrosis transmembrane conductance regulator (CFTR) $Cl^-$ channel, the protein that is defective in cystic fibrosis (CF), is also highly expressed in the kidney and is present in all segments of the rat nephron (Morales et al., 1996). CFTR expression is correlated with a cAMP-regulated $Cl^-$ conductance in cortical and inner medullary collecting duct cells (Vandorpe et al., 1995; Husted et al., 1995; Letz & Kormacher, 1997; Boese et al., 2000), and distal bright convoluted tubule cells (Ruberra et al., 1999). CFTR activation also leads to $Cl^-$ secretion in epithelial layers of collecting duct cells (Kizer, Lewis & Stanton 1995; Kizer et al., 1995*b;* Vandorpe et al., 1995; Boese et al., 2000). However, most of this work has been performed on model cell lines which by their very nature introduce some uncertainty as to the exact physiological relevance of the results. Indeed, using intact IMCD, Stanton (1989) could not show any discernible $Cl^-$ conductance in either luminal or peritubular membranes, although these experiments were performed in the absence of agonists. Despite these uncertainties, there is some evidence for a functional role for CFTR in the kidney, and yet a profound deficit in renal function is not observed in CF patients (*see* Simmons, 1993). A rationale for understanding this observation is that the severity of organ disease in CF correlates with the expression of an alternative $Cl^-$ conductance which functionally compensates

for loss of CFTR activity. Strong evidence exists from studies on transgenic CF mice, that this alternative pathway is likely to be a $Ca^{2+}$-activated $Cl^-$ conductance (Clarke et al., 1994; Gray et al., 1994; Winpenny et al., 1995; Kent et al., 1997). However, the presence of $Ca^{2+}$-activated $Cl^-$ channels (CaCC) in renal cells has only recently been addressed (Atia, Zeiske & Van Driessche, 1999; Boese et al., 2000; Cuffe et al., 2000), and the exact role these channels play in renal fluid and electrolyte transport is not fully established.

Recent molecular studies have provided a basis for improving our understanding of the role of CaCC in epithelial function. Cunningham et al. (1995) first described a full-length cDNA encoding an epithelial $Cl^-$ channel from bovine trachea, that encoded an ionomycin-stimulated $Cl^-$ conductance when transfected into COS-7 cells. Gandhi et al. (1998) used homology cloning to identify a mouse homologue (mCLCA1) that was expressed in heart, lung, liver and the kidney. When transfected into HEK293 cells, mCLCA1 expression conferred a time- and voltage-independent $Cl^-$ conductance with an outwardly rectifying current-voltage relationship after elevation of intracellular $Ca^{2+}$. Subsequent to this, Romio et al. (1999) identified a murine EST (mCaCC) containing a full-length cDNA that was essentially identical to mCLCA1. When transfected into *Xenopus* oocytes, mCaCC expression was associated with an outwardly rectifying, time-independent $Cl^-$ current, but the activity of this current did not require any increase in intracellular calcium. Other work has now identified three human CLCA homologues, and it is likely that these represent a family of closely related genes (Gruber et al., 1998*a*, 1999, Gruber, Gandhi, & Pauli, 1998; Gruber & Pauli, 1999), with at least two of the genes (CLCA1 and 2), coding for calcium-activated $Cl^-$ channels or channel regulators.

Our previous studies (Shindo, Simmons & Gray, 1996) have focused on the $Cl^-$ channels present in cells from the inner medullary collecting duct. Since this portion of the nephron determines the final composition of urine it is involved in significant transcellular anion transport and has to adapt to a wide range of extracellular conditions (Zeidel, 1993). In nephrolithiasis, the luminal anion composition and concentration in this segment are also critical predisposing factors for $Ca^{2+}$-crystal formation (Hojgaard & Tiselius, 1999) which further highlights the potential importance of anion transport in this segment. Our work used the mouse mIMCD-3 cell line that is known to retain some of the properties of the segment from which it originated (Rauchman et al., 1993). Using the 'fast' whole-cell configuration of the patch-clamp technique, we demonstrated that the basic electrophysiological properties of mIMCD-3 cells were unusual in that they displayed a very high resting $Cl^-$ conductance (Shindo et al., 1996). Furthermore, the majority of mIMCD-3 cells possessed $Cl^-$ currents that were both time and voltage-independent, and which gave an outwardly rectifying *I/V* relationship, properties very similar to those recently described for CLCA1 and 2 (Gandhi et al., 1998; Gruber et al., 1998*b*, 1999; Romia et al., 1999). However, in our original study we were unable to show any regulation of the resting $Cl^-$ conductance by $Ca^{2+}$ (Shindo et al., 1996). Since a significant disadvantage of conventional whole cell recordings is the disruption of the endogenous intracellular calcium-buffering systems of the cell, we decided to study the $Cl^-$ currents of IMCD cell using the 'slow' whole cell perforated patch technique (Horn & Marty, 1988) to overcome this problem.

Here we demonstrate that using perforated patch recordings, mIMCD-3 cells possess a substantial resting $Cl^-$ permeability that is precisely regulated by calcium. These basal whole cell currents could be inhibited or activated by variations in the $Ca^{2+}$ concentration of the bathing solution. Using dual-excitation microfluorimetry, changes in external calcium were associated with alterations in the free cytosolic calcium concentration ($[Ca^{2+}]_i$) of mIMCD-3 cells. In addition, mobilization of $[Ca^{2+}]_i$ by extracellular nucleotides also led to an increment in $Cl^-$ conductance showing that a variety of physiological stimuli modulate these $Ca^{2+}$-activated $Cl^-$ channels. Furthermore, RT-PCR analysis found expression of multiple mCLCA1-related transcripts which, combined with our pharmacological studies, suggests that mIMCD-3 cells may contain more than one type of CaCC. Our findings establish a novel link between alterations in external $Ca^{2+}$ and the activity of $Ca^{2+}$-activated $Cl^-$ transport in these cells. We speculate that changes in anion transport via the calcium-leak pathway and a calcium-sensitive apical $Cl^-$ conductance would provide a coordinated mechanism for regulating luminal anion composition and $Ca^{2+}$-crystal formation. Preliminary reports of some of the present data have been presented (Glanville et al., 1999; Stewart et al., 1999).

## Materials and Methods

### Cell Culture

mIMCD-3 cells (Rauchman et al., 1993) were kindly provided by Dr. S. Gullans (Brigham and Womens Hospital, Boston, MA), and were routinely cultured (passages 8–30) in Hams F12/DMEM (50/50% v/v) with 1 g/l D-glucose, 2 mM L-glutamine and 60 mg/ml gentamicin supplemented with 10% v/v foetal bovine serum at 37°C in an air/5% $CO_2$ atmosphere. For experiments cells were seeded at $3.5 \times 10^3$ cells/$cm^2$ on to 13 mm diameter glass coverslips and used 1–3 days later. mIMCD-K2 cells (passage 18) and T84 cells (passage 51) were cultured as described previously (Boese et al., 2000).

### Whole Cell Patch Recording

Current recordings were made using the whole cell, nystatin perforated patch recording technique (Horn & Marty, 1988) from confluent mono-

layers of mIMCD-3 cells perfused at 5 to 6 ml · $min^{-1}$. Whole-cell currents were recorded at 30°C with borosilicate glass electrodes (tip resistances 2–5 MΩ) with an EPC-7 patch-clamp amplifier (List Electronic, Darmstadt, Germany) using two voltage-clamp protocols. (i) During continuous recording, the membrane potential was held at 0 mV and then alternately clamped to ±60 mV for 1 sec. Between each pulse there was a 1 sec interval at the holding potential. (ii) To obtain current-voltage (*I/V*) relationships the membrane potential was held at 0 mV and then clamped over the range ±100 mV in 20 mV steps. Each voltage step lasted 500 msec, with an 800 msec interval at the holding potential between steps. Data were filtered at 1 kHz and sampled at 2 kHz with a Cambridge Electronic Design 1401 interface (CED, Cambridge, UK), and stored on either a digital tape recorder or the computer hard disk. When constructing *I/V* plots current measured 300 msec into the voltage pulse was used. Series resistance ($R_s$) was typically 3 times the pipette resistance, and $R_s$ compensation (40 to 70%) was routinely used. Membrane potentials ($V_m$) have been corrected for current flow ($I$) across the uncompensated fraction of $R_s$ using the relationship: $V_m = V_p - IR_s$, where $V_p$ is the pipette potential. Junction potentials were calculated using the JPCalc program (JPCalc v.2.02., P.H. Barry) and the appropriate corrections applied to $V_m$. Reversal potentials ($E_{rev}$) and conductance data were calculated from *I/V* plots by interpolation after fitting a fourth order polynomial using least squares regression analysis. Permeability ratios were derived from $E_{rev}$ values using the Hodgkin-Katz modification of the Goldman equation (Gray et al., 1990). Input capacitance was measured using the EPC-7 amplifier and values used to calculate current density as pA/pF.

## Measurements of Intracellular $Ca^{2+}$

mIMCD-3 cells grown on coverslips were loaded with Fura-2 by incubation for 35–50 min at 37°C in standard growth media containing 5 μM Fura-2/AM. The cells were then washed 3 times in bathing solution (*see below*) before the coverslip was fitted into the stage of an inverted microscope (Nikon, UK). The cells were imaged using an oil immersion lens (Nikon, Fluor 40 n.a. 1.3), and perfused continuously (bath volume 0.5 ml, perfusion at 2 ml/min). Changes in intracellular $Ca^{2+}$, $[Ca^{2+}]_i$, were determined by measuring the fluorescence of Fura-2 loaded cells with a dual-excitation wavelength microfluorimeter (Life Science Resources, UK). Groups of cells (3–5) were illuminated alternately at 340 nm and 380 nm using a rotating filter wheel, and emitted light was filtered using a 520 nm long-pass filter. Fluorescence data were corrected for background but not cell autofluorescence (typically 5% of Fura-2 intensity) and the emission ratio at the two excitation wavelengths ($R$) was determined as an index of intracellular $Ca^{2+}$ (Grynkiewicz, Poenie & Tsien, 1985). Records of $[Ca^{2+}]_i$ are displayed as the uncalibrated Fura-2 fluorescence ratio. We have deliberately not attempted to convert ratio values into $[Ca^{2+}]_i$, because of the difficulties in obtaining an accurate *Kd* value for the dye inside cells.

## Reverse Transcriptase-Polymerase Chain Reaction (RT-PCR)

Confluent cell layers (mIMCD-3, mIMCDK2, T84) were washed (×3) with phosphate buffered saline (PBS, 2.7 mM KCl, 1.47 mM $KH_2PO_4$, 137 mM NaCl, 8 mM $Na_2HPO_4 \cdot 7H_2O$). Lysis buffer (5 ml, 200 mM NaCl, 200 mM Tris-HCl pH 7.5, 1.5 mM $MgCl_2$, 4.7 μM disodium EDTA, 2% SDS, 1 μg proteinase K) was added and layers were incubated for 5–10 min at 20°C. The resultant lysate was titurated through a 21-gauge needle, transferred to a 20 ml universal tube and incubated at 45°C for 1 hr. Sodium chloride was added to a final concentration of 300 mM before resuspension, as above.

mRNA was purified from total RNA by the use of an oligo-dT resin method (Pharmacia Biotech, St. Albans, Herts, UK). Poly-$A^+$ RNA was precipitated by the addition of 40 μl of 3 M sodium acetate pH 5.2 (Sigma) and 1 ml of 100% ethanol (BDH, Analar). After centrifugation (30,000 × $g$ for 1 hr 4°C) the solution was decanted and the pellet air-dried for 5 min before adding 100 μl of Tris-HCl, pH 8.5. This was incubated at 65°C for 10 min to aid dissolution. Purity and yield of mRNA was assessed by absorbance at 260 nm and 280 nm.

Samples of poly-$A^+$ RNA (1 μg) were incubated with RT buffer (50 mM Tris-HCl pH 8.3, 50 mM KCl, 4 mM $MgCl_2$, 10 mM DTT, MBI Fermentas), 0.5 mM dNTPs (MBI Fermentas), 10 units Moloney murine leukaemia virus reverse transcriptase (M-MuLV RT MBI Fermentas), 20 units RNase inhibitor (MBI Fermentas) and 0.023 units random hexamer primers (Pharmacia Biotech). Total volume was 20 μl, made with water (molecular biology grade, BDH), and incubation was at 42°C for 1 hr. Negative controls were included where M-MuLV RT was omitted to discount false positives due to DNA contamination. cDNAs (2.5 μl in a 25 μl PCR reaction) were incubated with PCR buffer (10 mM Tris-HCl pH 8.8, 50 mM NaCl, 0.08% Nonidet P40, MBI Fermentas), 2 mM $MgCl_2$ (MBI Fermentas), 0.2 mM dNTPs, 1.25 units recombinant *Taq* DNA polymerase (MBI Fermentas), 0.5 μM forward and reverse primers and molecular biology grade water (BDH). PCR was performed using the PCR Express Thermal Cycler (Hybaid) for 30 amplification cycles. Each cycle consisted of 94°C for 30 sec, 55°C for 30 sec, and 72°C for 60 sec. Oligonucleotide primers for mCLCA1 (mCACC) were from the published mouse mCLCA1 sequence; forward primer 5′-GCCTCCATAATGTTCATGC-3′, reverse primer, 5′-CCGGAAGTGCTCGGTCAC-3′ as described by Gruber et al. (1998*b*). Oligonucleotide primers for CFTR were taken from Morales et al., (1996); forward primer 5′-AAAAAAGGAAGAATTCTATTCT-3′, reverse primer 5′-CTAAGCACCAAATTAGCAC-3′. This allows detection of full-length and truncated CFTR isoforms (Morales et al., 1996). PCR products were analyzed using agarose gel electrophoresis of PCR mixtures, using ethidium bromide fluorescence to visualize products. Appropriate gel bands were excised from the gel and cloned using the TA cloning vector pCR2.1 TOPO (Invitrogen). The identity of the cloned PCR products was determined by automatic sequencing using fluorescent di-deoxy dye-termination on an ABI Prism model 377 automated sequencer. Comparison of the identity of the cloned PCR fragments to published sequence was performed using BLASTN (www.ncbi.nlm.nih.gov) (Altschul et al., 1997).

## Solutions and Chemicals

The standard pipette solution contained (mM): 130.0 KCl, 10 NaCl, 2.0 $MgCl_2$, 10.0 HEPES and Nystatin (100–300 μM) pH 7.2 (with TRIS). The osmolarity of this solution was 230 mosmol/l. The standard $Na^+$-rich bath solution used for electrophysiology and fluorescence measurements contained (mM): 137.0 NaCl, 0.3 $NaH_2PO_4$, 5.4 KCl, 0.3 $KH_2PO_4$, 2.8 $CaCl_2$, 1.2 $MgSO_4$, 5.0 glucose, 14.0 TRIS base, pH 7.4 (with HCl). The osmolarity of this solution was 300 mosmol/l. For the anion-replacement studies 100 mM NaCl in the standard bath solution was replaced by 100 mM sodium salt of another anion, or by 185 mM mannitol for the reduced NaCl bath solution. A low $Ca^{2+}$ bath solution was made by omitting calcium from the standard bath solution (estimated free calcium concentration <100 μM). A divalent-free bath solution was made by omitting $Ca^{2+}$ and $Mg^{2+}$ from the standard bath solution. We found that EGTA-based bath solutions caused the activation of a cation conductance and therefore we could not assess the effect of lower calcium concentrations in these cells. Ionomycin, DIDS (4,4′-diisothiocyanatostilbene-2,2′-disulphonic acid), niflumic acid, glybenclamide and NPPB (5-nitro-2-(3-phenylpropylamino)benzoate (TOCRIS, Bristol, UK) were made up as 10–100 mM stock solutions in

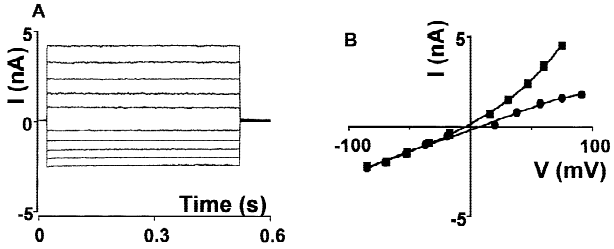


**Fig. 1.** Characteristics of basal chloride currents in mIMCD-3 cells. (*A*) Whole cell currents elicited by the ±100 mV voltage protocol described in Materials and Methods. (*B*) Current-voltage (*I/V*) plot for the data in *A.* Squares, *I/V* plot with standard bath solution. Circles, *I/V* plot after changing to reduced NaCl solution in the bath (*see* Materials and Methods for details of composition of solutions).

dimethylsulphoxide (DMSO) and then diluted to the required concentration. Nystatin (Calbiochem), used in the slow whole cell experiments, was made up as 40 mM stock solutions in DMSO and then diluted in pipette solution to a working concentration of 150–300 μM. DTT (dithiothreitol) and ATP were dissolved directly in the standard bath solution. In some of the ATP experiments a 'fast perfusion' system (DAD-12, Digitimer, UK) was employed to expose cells to ATP. This system has an exchange time of less than 1 sec. BAPTA-AM and FURA2-AM were from Molecular Probes, Oregon. Unless otherwise stated all chemicals were from Sigma.

### Statistics

Data are expressed as mean ± SE. Significance of difference between mean values of two groups was tested by Student's *t* test (paired or unpaired, as appropriate). Alternatively, for multiple comparisons between control and treatment groups, data were analyzed using one way analysis of variance (ANOVA), followed by Tukey-Kramer multiple comparison test. A probability of $P < 0.05$ was considered significant.

## Results

### Properties of Basal Whole Cell Currents in mIMCD-3 Cells

Our previous fast whole cell patch clamp studies identified a large, outwardly rectifying $Cl^-$ conductance in mIMCD-3 cells (Shindo et al., 1996). However, in our original paper we were unable to show any acute regulation of this $Cl^-$ current by changes in either intra- or extracellular calcium. To investigate whether the lack of regulation by calcium, and the high basal activity, were in some way associated with the fast whole cell recording technique employed in these early studies, we performed experiments using the nystatin perforated patch technique first described by Horn and Marty (1988).

In the absence of any stimulants, we again found that the majority of mIMCD-3 cells (190/298) possess a large, spontaneously active, $Cl^-$ conductance (Fig. 1*A*), indicating that the high basal activity is not dependent on recording configuration. However, the currents measured using perforated patch recordings were found to be more stable than those obtained from fast whole cell recordings. Under fast whole cell recording conditions, currents decline by over 60% during the first 15 min of experiments, whereas slow whole cell currents were stable over this period (fast whole cell: initial current density 201 ± 30 pA/pF; after 15 min, 60 ± 9 pA/pF, $n = 6$: slow whole cell: initial current density, 169 ± 23 pA/pF; after 15 min, 167 ± 21 pA/pF, $n = 6$). Over the potential range of ±100 mV Fig. 1*A* shows that the basal currents measured with perforated patch recordings show no time- or voltage-dependence. The current-voltage (*I/V*) plot (Fig. 1*B*) shows clear outward rectification with a negative reversal potential. Overall, from 190 cells the reversal potential ($E_{rev}$) was −9.6 ± 0.5 mV, a value relatively close to the predicted equilibrium potential for chloride under our experimental conditions (−2.2 mV), assuming complete equilibration of $Cl^-$ through the nystatin pores (Horn & Marty, 1988). With standard bath conditions the current densities were 272 ± 13 and 176 ± 8 pA/pF when measured at $E_{rev}$ ± 60 mV, a value significantly higher than our previous measurements (66 ± 5 and 44 ± 3 pA/pF Shindo et al., 1996). Lowering external NaCl from 137 to 37 mM (maintaining osmolarity with mannitol), shifted the $E_{rev}$ by 15.5 ± 0.5 mV ($n = 33$), giving a $P_{Na}/P_{Cl}$ of 0.23 ± 0.01 (*see* Fig. 1*B*). Replacing 100 mM external NaCl with 100 mM Na aspartate shifted the $E_{rev}$ by 19.9 ± 0.6 mV ($n = 13$), while a similar replacement with NaI caused a negative shift of −3.7 ± 1.0 mV ($n = 5$), giving a calculated $P_{Asp}/P_{Cl}$ of 0.15 ± 0.02 and a $P_I/P_{Cl}$ of 1.3 ± 0.1. Overall, apart from current density, these results are very similar to our previous measurements (Shindo et al., 1996), and indicate that perforated patch recordings do not alter markedly the biophysical properties of this outwardly rectifying current.

### Pharmacological Inhibition of Basal mIMCD-3 $Cl^-$ Currents

Our previous studies on the outwardly rectifying $Cl^-$ conductance of mIMCD-3 cells using fast whole cell recordings (Shindo et al., 1996), found that the current was effectively inhibited by 100 μM glybenclamide and NPPB when added extracellularly, but was only partially blocked by DIDS even at high concentrations. More recently it has been shown that mCLCA1/mCaCC (Ghandi et al., 1998; Romio et al., 1999) as well as human CLCA1 and 2 (Gruber et al., 1998*a*, 1999) were effectively inhibited by DIDS at concentrations between 100–300 μM, and were also sensitive to niflumic acid and DTT. We therefore tested the ability of these compounds to inhibit the basal $Cl^-$ currents in mIMCD-3 cells. Figure 2 shows that in the presence of 2 mM ex-

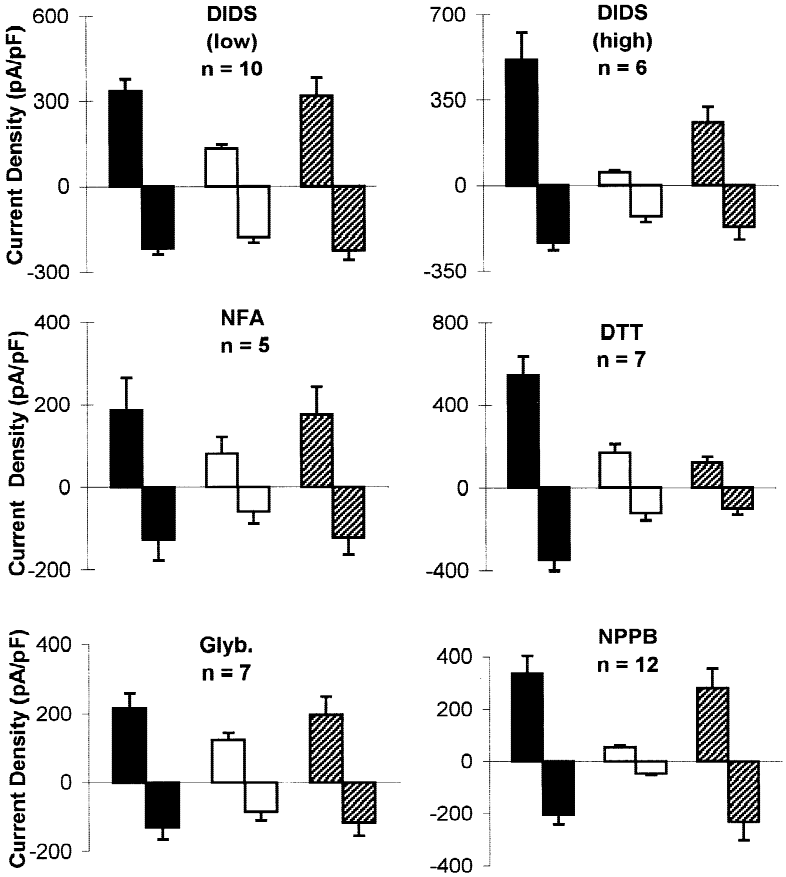


**Fig. 2.** Effect of channel blockers on basal chloride currents in mIMCD-3 cells. Summary of the inhibition by different blockers. Results are expressed as current density measured at $E_{rev}$ + 60 mV (upper columns) and $E_{rev}$ − 60 mV (lower columns), for controls (solid bars), in the presence of blocker (open bars) and after washout of inhibitor (hatched bars). Low DIDS, 100 μM DIDS; High DIDS, 500 μM DIDS; NFA, 100 μM Niflumic Acid; 5 mM DTT; Glyb, 100 μM glybenclamide and NPPB, 100 μM.

ternal calcium, the basal $Cl^-$ currents were sensitive to all compounds when applied to the extracellular solution ($P < 0.01$, ANOVA), with the block by DIDS alone showing any significant voltage-dependence. The percentage block caused by the inhibitors was as follows: 100 μM DIDS, 59 ± 5% ($n = 10$); 500 μM DIDS, 87 ± 4% ($n = 6$); 100 μM niflumic acid, 61 ± 6% ($n = 5$), 5 mM DTT, 70 ± 6% ($n = 7$); 100 μM glybenclamide, 59 ± 13% ($n = 3$), and 100 μM NPPB, 87 ± 4% ($n = 4$), when measured at $E_{rev}$ + 60 mV. The block by 100 μM DIDS, niflumic acid, glybenclamide and NPPB was fully reversible, whereas complete reversal was not observed at the higher DIDS concentration, and no reversal was ever observed for DTT block, even after extensive washing (*see* Fig. 2 and 9), similar to the findings reported by Ji et al. (1998). Clearly, the present inhibitor data for DIDS, niflumic acid and DTT are very similar to the results reported for mCLCA1/mCaCC (Gandhi et al., 1998; Romio et al., 1999). However, the magnitude of the block by DIDS in these slow whole cell recordings is significantly greater than we previously reported (Shindo et al., 1996), although in both cases block displayed a similar voltage-dependence (greater at positive $V_m$). The reason for this discrepancy is not known, but it may indicate that DIDS block is dependent on recording configuration, or that the channel sensitivity has changed. Nonetheless, apart from the extent of DIDS block, we conclude that the biophysical and pharmacological properties of the outwardly rectifying $Cl^-$ conductance are similar under fast and slow whole cell recording conditions.

## Regulation of Basal Currents by Calcium

Since the outwardly rectifying $Cl^-$ currents were spontaneously active this suggested that the underlying channels were open at the normal resting calcium levels found in these cells. To investigate this further the free cytosolic calcium concentration ($[Ca^{2+}]_i$), was reduced by preloading the cells with BAPTA-AM (30 μM), a membrane permeant calcium buffer, for 1 hr. This significantly reduced current density by approximately 40%. For control (unloaded) cells studied at the same time, current density was 265 ± 25 and 173 ± 19 pA/pF ($n = 24$) and for the BAPTA-loaded cells it was 155 ± 31 and 98 ± 17 pA/pF ($n = 20$, $P < 0.05$, unpaired *t*-test). For the BAPTA-loaded cells the whole cell currents also had a more negative $E_{rev}$ (−23.2 ± 3.6 mV *vs.* −8.9 ± 2.1 mV, $P < 0.0001$, unpaired *t*-test), indicating a reduction

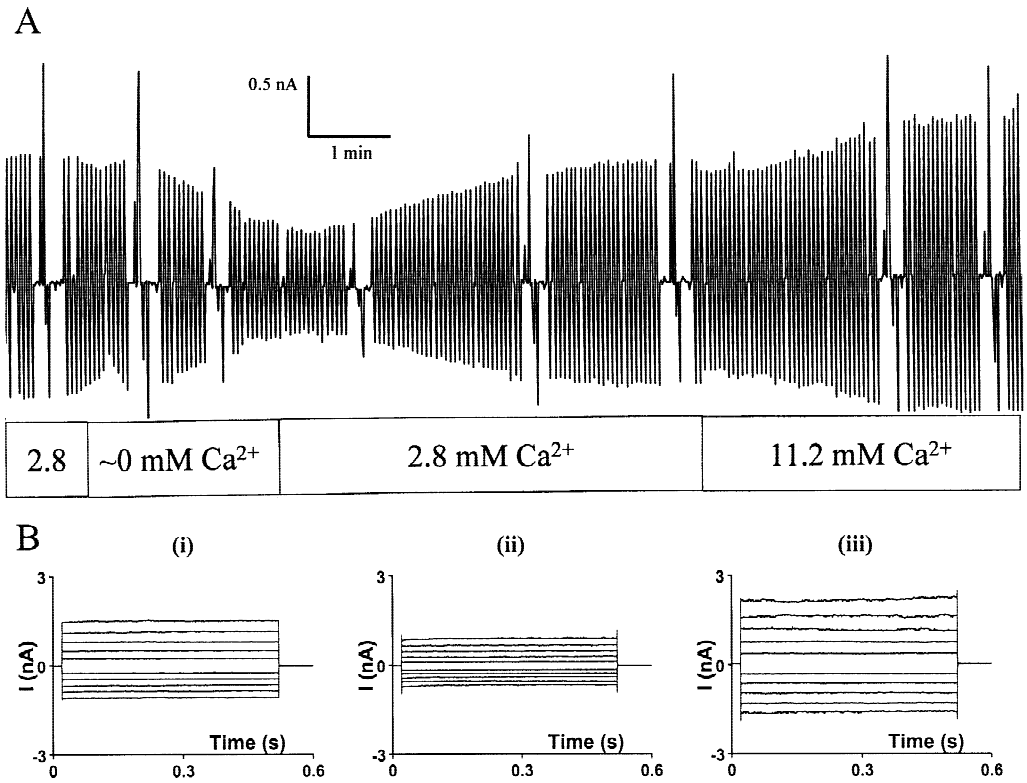


**Fig. 3.** Regulation of basal currents by extracellular calcium. (*A*) Continuous whole cell recording showing the effect of extracellular calcium concentration on the size of basal currents, monitored using the ±60 mV voltage protocol described in Materials and Methods. (*B*) Whole cell currents elicited by the ±100 mV voltage protocol at different extracellular calcium concentrations (i) 2.8 mM (ii) nominally calcium-free (iii) 11.2 mM.

in whole cell $Cl^-$ selectivity. We then investigated whether changes in external calcium could also regulate the conductance via a change in $[Ca^{2+}]_i$. Lowering the extracellular calcium concentration from 2.8 mM (standard conditions) to μM levels (nominally calcium-free solution, *see* Materials and Methods) reduced current density from 265 ± 25 and 173 ± 19 pA/pF to 155 ± 31 and 98 ± 17 pA/pF ($n = 4$, $P < 0.05$, paired *t*-test). Note that we could not test the effects of reducing extracellular calcium to submicromolar levels, (using EGTA), as this resulted in the activation of very large cation-selective currents, similar to those described by Korbmacher et al. (1995) in M-1 mouse CCD cells.

We then went on to investigate the response of the IMCD-3 cells to alterations in extracellular $Ca^{2+}$ in more detail. Figure 3*A* shows the effect of multiple changes in external $Ca^{2+}$ on the size of the whole cell currents. Note that both a decrease and increase in external $Ca^{2+}$ are associated with slow, monophasic, changes in whole cell conductance (Fig. 3*A*). Overall, the time for the changes in whole cell current to reach a steady-state level was 141 ± 16 sec ($n = 18$). Figure 3*B* illustrates the biophysical properties of the whole cell currents obtained after changing to the low (3Bii) or high (11.2 mM) external calcium concentrations (3Biii). It is clear from these data that the properties of the currents are essentially identical to those measured with 2.8 mM external calcium (3Bi). In addition, current reversal potentials were also similar (low calcium: −2.7 ± 2.6 mV ($n = 4$); high calcium −4.6 ± 1.4 mV ($n = 6$); standard −5.5 ± 1.0 mV ($n = 18$), making it likely that only the outwardly rectifying $Cl^-$ conductance was being modulated by changes in external calcium concentration. Figure 4 shows that the effect of external calcium is clearly dose-dependent, with whole cell $Cl^-$ current density reaching a maximum at an external calcium concentration of ~5–6 mM (Fig. 4). The maneuvers described above indicated that external calcium modulated the size of the basal currents, and we speculated that this was due to changes in $[Ca^{2+}]_i$. To test for this directly, mIMCD-3 cells were loaded with the calcium-sensitive dye FURA-2 (*see* Materials and Methods) and exposed to bath solutions containing different levels of calcium.

Figure 5*A* shows the response of mIMCD-3 cells to multiple changes in external calcium over a similar time course to that used for the whole cell current experi-

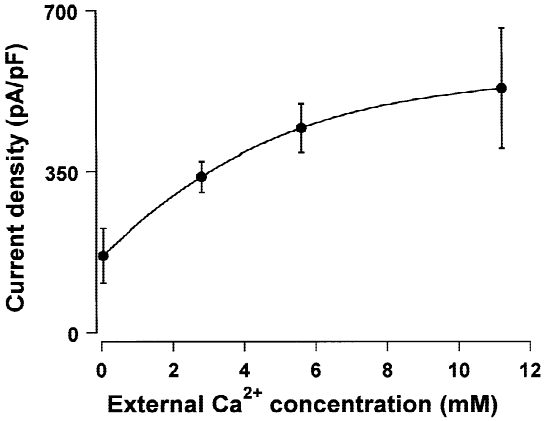


**Fig. 4.** Dose-response curve for extracellular calcium concentration. Current data measured at $E_{rev}$ + 60 mV. Values represent mean ± SEM from between 4–18 experiments for different calcium concentrations.

ments. Reducing the standard extracellular calcium concentration from 2.8 mM to μM levels (nominally calcium-free) results in a clear reduction in $[Ca^{2+}]_i$. Shifting from 2.8 to 11.2 mM external calcium had the opposite effect and produced an increase in fluorescence ratio. Similar results were observed in 3 other experiments. These results illustrate that the resting $[Ca^{2+}]_i$ is clearly dependent on the prevailing external calcium concentration, and strongly suggest that the changes in current size associated with alterations in external calcium illustrated in Figs. 3 and 4, are due to alterations in resting $[Ca^{2+}]_i$. An important feature to notice is that the monophasic changes in $Cl^-$ currents observed in Fig. 3 are mirrored by similar changes in $[Ca^{2+}]_i$, (Fig. 5). No rapid or transient effects in $[Ca^{2+}]_i$ were observed on changing to different external calcium solutions. Recently, similar slow changes in $[Ca^{2+}]_i$ have been observed in isolated pancreatic ducts (Bruce et al., 1999) exposed to varying external calcium concentrations. These authors showed that the changes in $[Ca^{2+}]_i$ were linked to the activation of a cell surface $Ca^{2+}$/polyvalent cation receptor (CaR). To investigate whether a CaR was also involved in the responses observed in our studies, we exposed mIMCD-3 cells to neomycin in a bath solution containing 0.5 mM calcium. Figure 5*B* shows that 1 mM neomycin ($n = 3$), produced no change in $[Ca^{2+}]_i$, even though a subsequent exposure to ATP did mobilize intracellular stores. In addition, exposing cells to 0.6 or 1.0 mM $Gd^{3+}$, ($n = 10$ for both concentrations) in a divalent-free bath solution (Bruce et al., 1999) also failed to produce any clear increase in $[Ca^{2+}]_i$ (Fig. 5*C*). Overall, the pattern of changes in $[Ca^{2+}]_i$, together with the pharmacological evidence, suggest that the coupling between external calcium and plasma membrane $Cl^-$ conductance is not mediated via a CaR, but involves a plasma membrane calcium-permeable pathway.

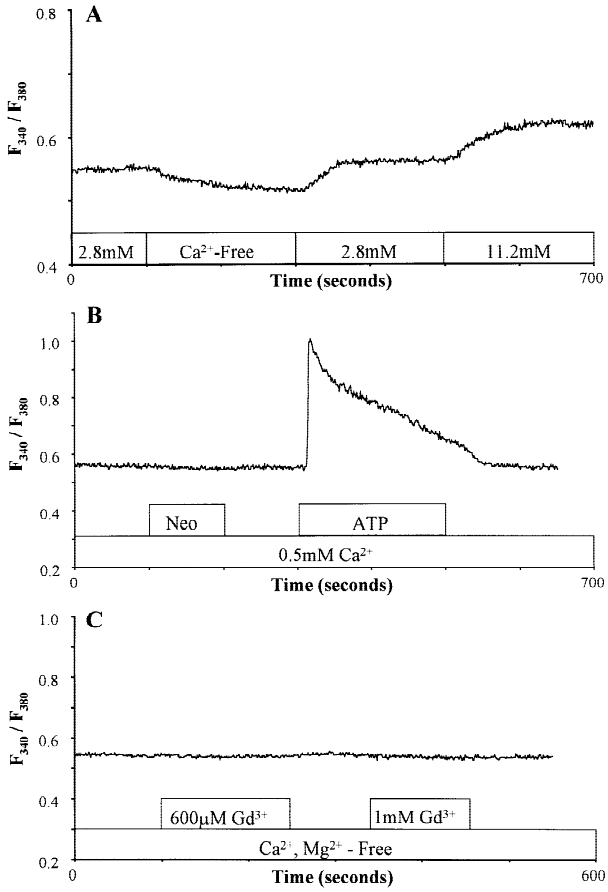


**Fig. 5.** Changes in external calcium modulate intracellular calcium levels. (*A*) Effect of reducing bath calcium concentration on FURA-2 fluorescent ratio (340 nm/380 nm). (*B*) Failure of 1 mM neomycin to effect $[Ca^{2+}]_i$. Measurements were performed in a bath solution containing 0.5 mM $Ca^{2+}$ (Bruce et al., 1999). Trace also shows that extracellular ATP (100 μM) was able to mobilize calcium after neomycin exposure (*C*) Failure of $Gd^{3+}$ to affect $[Ca^{2+}]_i$. The effect of $Gd^{3+}$ was assessed in a divalent-free bath solution (Bruce et al., 1999).

## ATP Stimulation of Whole Cell Currents in mIMCD-3 Cells

The results depicted in Figs. 3 and 4 suggested that changes in $[Ca^{2+}]_i$ were able to modulate the size of the basal $Cl^-$ currents. To investigate the role of $[Ca^{2+}]_i$ further the effect of exposing mIMCD-3 cells to extracellular ATP was tested, since activation of purinergic receptors has recently been shown to stimulate $Cl^-$ secretion in the mIMCD-K2 cell line (McCoy et al., 1999; Boese et al., 2000). Figure 6 shows that ATP (100 μM) caused a marked increase in whole cell conductance. Currents reached a steady-state value after 191 ± 29 sec exposure to ATP ($n = 12$) with normal bath perfusion, or after 147 ± 19 sec ($n = 9$) with a fast perfusion system (*see* Materials and Methods). Figure 7*B* shows that the

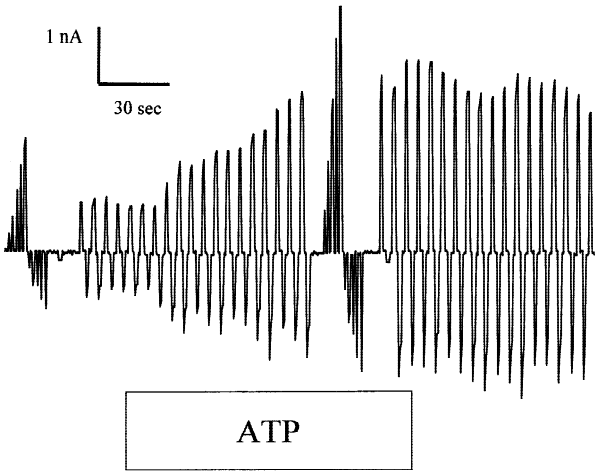


**Fig. 6.** Effect of extracellular ATP on basal currents. Continuous recording showing the effect of 100 μM extracellular ATP on basal $Cl^-$ currents, monitored using the ±60 mV protocol.

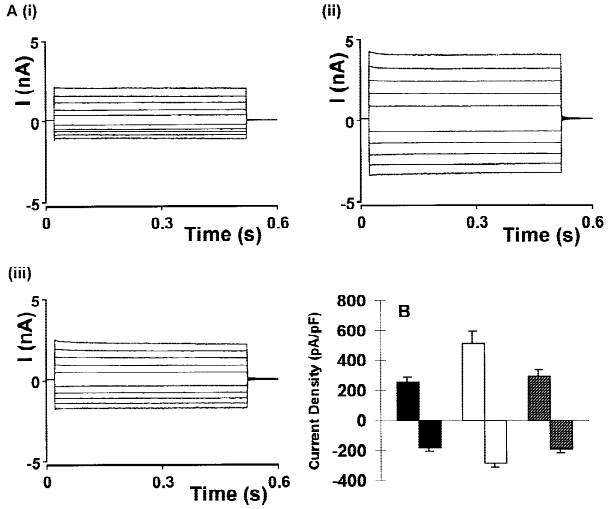


**Fig. 7.** Extracellular ATP stimulates whole cell currents. (*A*) Whole cell currents elicited by the ±100 mV protocol for (i) control, (ii) ATP-stimulated and (iii) after washout of ATP. (*B*) Summary of the effects of ATP on current density, measured at $E_{rev}$ ± 60 mV. Filled bars, initial currents; open bars, +ATP; stippled bars, after washout of ATP.

effect of ATP was fully reversible in twenty-one experiments studied. The ATP-activated currents were also time- and voltage-independent (Fig. 7*A*ii), with an outwardly rectifying *I/V* plot reversing at −5.3 ± 0.5 mV ($n$ = 61). From the reversal potentials it appears that ATP stimulation shifts $E_{rev}$ towards $E_{Cl}$. (−9.4 ± 0.8 mV to −5.3 ± 0.5 mV, $P < 0.01$, paired *t*-test). In addition, the ATP-activated currents had similar $P_{Na}/P_{Cl}$ values (0.25 ± 0.02, $n$ = 8) when compared to the basal currents. Overall, ATP increased current density in 61 cells tested from 241 ± 17 and 173 ± 12 pA/pF to 454 ± 39 and 281 ± 17 pA/pF at $E_{rev}$ ± 60 mV, respectively ($P < 0.001$, ANOVA). This stimulation was completely abolished in cells pretreated with BAPTA-AM (30 μM) for 1 hr, where the percentage increase was only 6 ± 6% and 6 ± 8% ($n$ = 8). In cells studied at the same time, but without the BAPTA pretreatment, ATP produced an increase of 112 ± 34% and 78 ± 20% ($n$ = 12) ($P < 0.05$, ANOVA). Increases in whole cell currents were also observed after exposure to ionomycin (100 nM), where mean current density rose from 280 ± 52 and 186 ± 33 pA/pF to 425 ± 68 and 250 ± 44 pA/pF respectively ($P < 0.05$, paired *t*-test, $n$ = 6). Although the ionomycin-stimulated currents appeared identical to those observed with ATP, the stimulation was generally irreversible with ionomycin.

To correlate the ATP-dependent increase in whole cell conductance with changes in $[Ca^{2+}]_i$, FURA-AM loaded cells were exposed to extracellular ATP (100 μM). Figure 8*A* shows a typical, biphasic, response to ATP observed in 14 separate experiments. Addition of ATP caused an initial peak in $[Ca^{2+}]_i$, that decayed to a plateau value, significantly above resting levels. The peak in $[Ca^{2+}]_i$ occurred after 21 ± 3 sec following ATP addition. Similar results have been reported for the effects of ATP on $[Ca^{2+}]_i$ from intact rat IMCD tubules (Ecelbarger et al., 1994). Figure 8*B* shows that preloading the cells with BAPTA-AM completely prevented any subsequent increase in $[Ca^{2+}]_i$ by ATP ($n$ = 5). Overall, the results in Figs. 3 and 6 demonstrate that a decrease or increase in $[Ca^{2+}]_i$ leads to similar directional changes in the size of the basal $Cl^-$ conductance, providing strong evidence that this current is regulated by intracellular calcium. However, the changes in intracellular $Ca^{2+}$ (*see* Figs. 5 and 8), particularly with ATP, occur more rapidly than the changes in current size which suggests that calcium per se is unlikely to directly gate the channel. Additional factors/pathways such as protein phosphorylation are likely to be involved.

### Inhibition of ATP-Stimulated $Cl^-$ Currents

In order to establish whether the same channel underlies both basal and nucleotide-stimulated currents, the effects of DIDS, niflumic acid, glybenclamide, NPPB and DTT were tested on the ATP-stimulated currents. DIDS, niflumic acid, glybenclamide and NPPB produced a similar amount of block to that observed for the basal currents ($P > 0.05$, ANOVA), the percentage inhibitions being; 100 μM DIDS, 37 ± 5% ($n$ = 7), 500 μM DIDS, 71 ± 5% ($n$ = 5), niflumic acid, 54 ± 12% ($n$ = 4), 100 μM glybenclamide, 42 ± 15% ($n$ = 3), and 100 μM NPPB, 75 ± 5% ($n$ = 5). Quite unexpectedly the response of the ATP-stimulated current to DTT was opposite to that observed for the basal currents ($P < 0.001$, ANOVA) as illustrated in Fig. 9*A* and *B*. Exposing cells to 5 mM DTT without

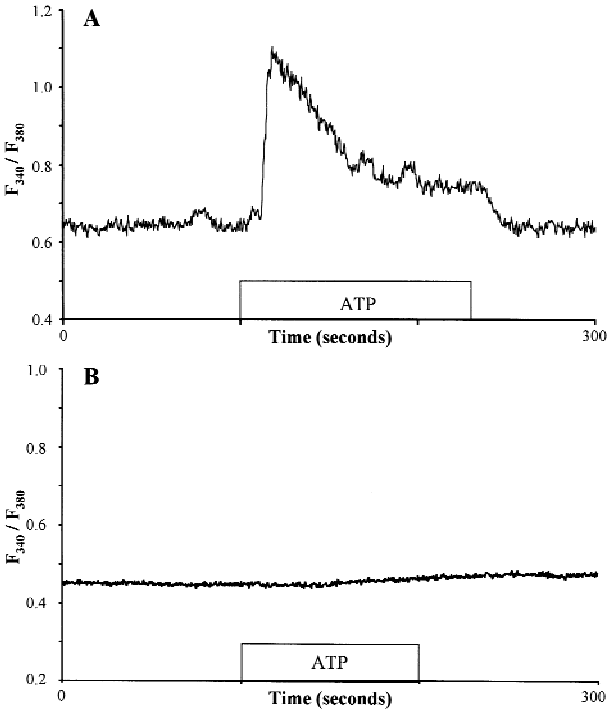


**Fig. 8.** Effect of extracellular ATP on intracellular calcium concentration. (*A*) Shows the effect on of exposing a control group of mIMCD-3 cells to 100 μM ATP on $[Ca^{2+}]_i$, while (*B*) illustrates the lack of effect of ATP on $[Ca^{2+}]_i$, after mIMCD-3 cells were pretreated for 1 hr with 30 μM BAPTA-AM.

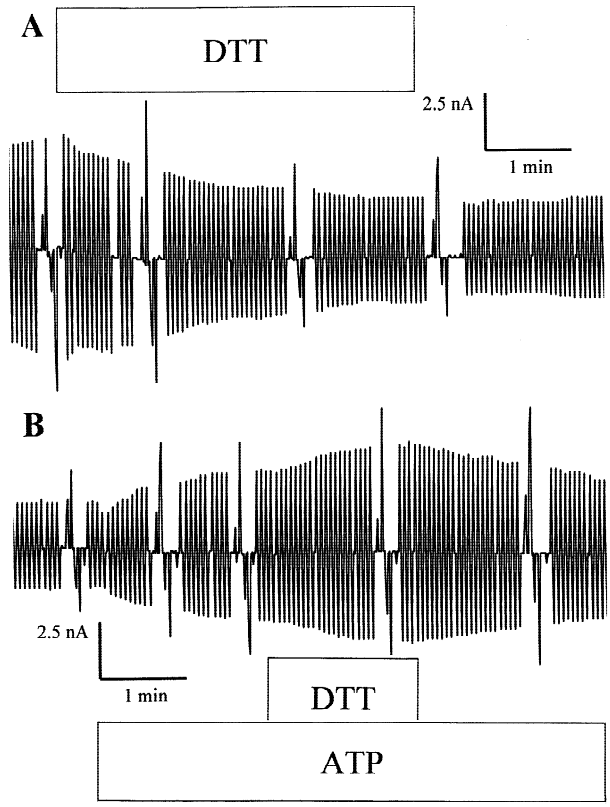


**Fig. 9.** Effect of DTT on basal and ATP-stimulated chloride currents. (*A*) Continuous recording showing the effect of 5 mM extracellular DTT on basal $Cl^-$ currents, monitored using ±60 mV protocol. (*B*) Continuous recording showing the effect of first, 100 μM extracellular ATP, followed by 5 mM DTT on whole cell $Cl^-$ currents.

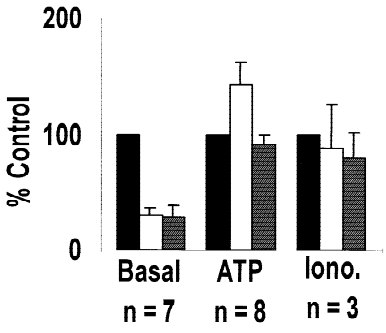


**Fig. 10.** DTT blocks basal but not ATP- or ionomycin-stimulated currents. Current density measured at $E_{rev}$ +60 mV and expressed as a percentage of control for, basal ($n = 4$), ATP-stimulated (100 μM, $n = 5$) and ionomycin-stimulated (0.1 μM, $n = 3$) currents after exposure to 5 mM DTT. Filled bars, initial basal currents; open bars, +DTT; stippled bars, after washout of DTT.

any ATP stimulation produced a clear irreversible block, as already described in Fig. 2. In contrast, if DTT was added to cells that had been first exposed to ATP, this caused a further increase in whole cell conductance, which was reversible on washout of the DTT (Fig. 9*B*). The biophysical properties of this DTT-stimulated current were similar to both the ATP-stimulated and basal currents and displayed similar selectivity ($P_{Na}/P_{Cl} = 0.31 \pm 0.06$, $n = 3$). In addition, subsequent removal of ATP after DTT exposure and washout led to the normal decline of whole cell currents to pre-agonist levels, indicating that DTT treatment had not altered the responsiveness of the $Cl^-$ conductance to calcium. However, ATP failed to cause an increase in current density if added to cells that had been first exposed to DTT ($n = 3$). Figure 10 summarizes the effects of DTT, and also shows that DTT had no significant effect on ionomycin-stimulated currents (87 ± 25% and 87 ± 14% of control values, $P > 0.05$, paired *t*-test, $n = 3$), a result in direct contrast to effects on basal currents. In separate experiments, the effect of DTT on $[Ca^{2+}]_i$ was also tested in the absence ($n = 3$) and presence of ATP ($n = 4$). Under both conditions DTT produced a transient increase in $[Ca^{2+}]_i$ (Fig. 11*A* and *B*), which indicates that changes in this parameter alone cannot explain the different responses of the basal and ATP-stimulated currents to DTT. In addition Fig. 11*A* also indicates that cells exposed first to DTT, are still able to respond to ATP, and mobilize intracellular calcium. This strongly suggests that once DTT has blocked the basal currents they can no

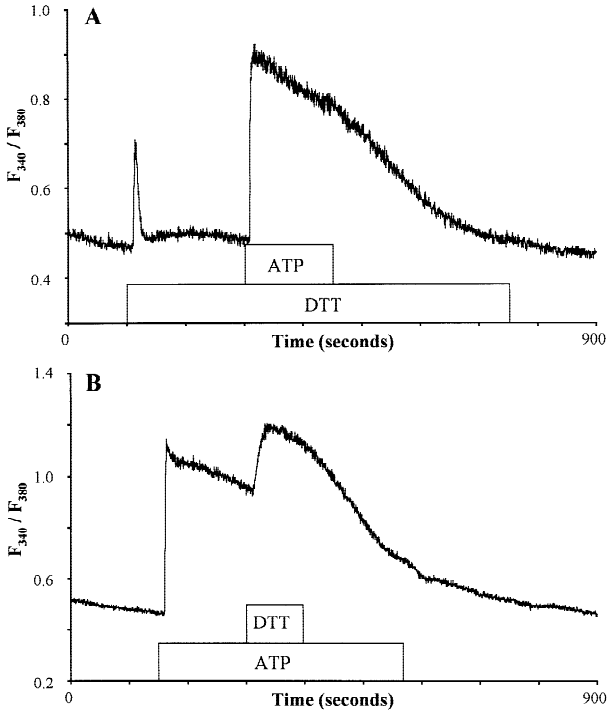


**Fig. 11.** Effect of DTT on intracellular calcium concentration. (*A*) The effect of 5 mM DTT on $[Ca^{2+}]_i$. DTT was added either before 100 μM extracellular ATP or (*B*) during an on-going exposure to 100 μM extracellular ATP.

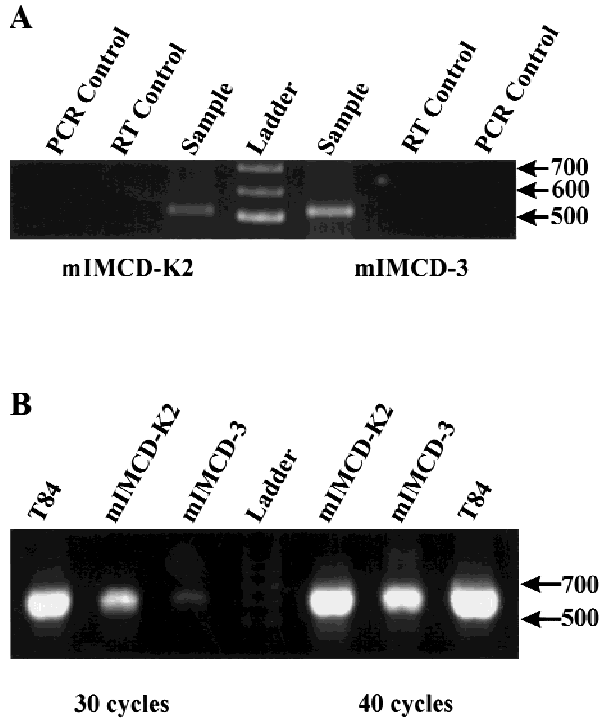


**Fig. 12.** Identification of mCLCA and CFTR mRNA expression in mIMCD-3 cells. (*A*) Ethidium-stained agarose gel showing RT-PCR products using mCLCA1 gene-specific primers. Lane 1: PCR control (water alone), Lanes 2: RT control (omitting reverse transcriptase). Lane 3: Positive control using mIMCD-K2 cells. Lane 4: Molecular size ladder. Lane 5: mIMCD-3 cell sample. Lanes 5 & 6: RT and PCR controls. (*B*) Ethidium-stained agarose gel showing RT-PCR products using CFTR gene-specific primers. Lane 1: positive control, T84 cell sample (30 cycles). Lanes 2: positive control, mIMCD-K2 cell sample (30 cycles). Lane 3: mIMCD-3 cell sample (30 cycles). Lane 4: Molecular size ladder. Lane 5: mIMCD-K2 cell sample (40 cycles). Lane 6: mIMCD-3 cell sample (40 cycles). Lane 7: positive control, T84 cell sample (40 cycles).

longer respond to changes in $[Ca^{2+}]_i$. Our conclusion is that the ATP-stimulated (and ionomycin-stimulated) currents have a distinct pharmacological profile compared to the basal currents.

## Molecular Identity of $Ca^{2+}$-Dependent Chloride Currents in mIMCD-3 Cells

Using gene-specific primers (Gruber et al., 1998*a*,*b*) to amplify reverse-transcribed mRNA, we identified a PCR product of ~518 bp consistent with mCLCA1 (mCACC) mRNA expression in mIMCD-3 cells (Fig. 12*A*), (Gandhi et al., 1998; Romio et al., 1999). As a positive control the mCLCA product from mIMCD-K2 cells is also shown (Boese et al., 2000). Note that equivalent amounts of mRNA were used for RT, and PCR reaction conditions were the same. Control reactions (minus cDNA or minus reverse transcriptase) confirm specificity and rule out any genomic DNA contamination. Figure 12*B* shows RT-PCR data for CFTR, which should produce an expected band of 510 bp. Although CFTR mRNA is readily detected in both mIMCD-K2 cells and in T84 cells (present as an additional positive control), only a very faint PCR product was detected for mIMCD-3 cells after 30 amplification cycles. However, after further 10 rounds of amplification a weak product was evident. Cloning and sequencing of multiple clones derived from the CLCA PCR product from mIMCD-3 cells produced 3 distinct, but related, sequences corresponding to products of 518 bp (mIMCD-3/1), 527 bp (3/2) and 481 bp (3/3). Figure 13 shows a multiple sequence alignment of the three mIMCD-3 PCR products, together with mCLCA1 and the mammary isoform, mCLCA2, for comparison (Accession numbers, AF047838 Gandhi et al., 1998, AF108501; Lee et al., 1999, respectively). For mIMCD3/1 (518 bp) there is 97.1% identity to mCLCA1 and 98.1% identity to mCLCA2 (Altschul et al., 1997). The second product mIMCD3/2, was not only distinct from mCLCA1 (82.5% identity) but also was different to mCLCA2, (82.5% identity). Notably there is a 9 bp insert in the 527 bp product present in neither mCLCA1 nor 2. The shorter PCR product (mIMCD-3/3) contains a 46 bp deletion when compared to mIMCD-3/2, but is otherwise identical.

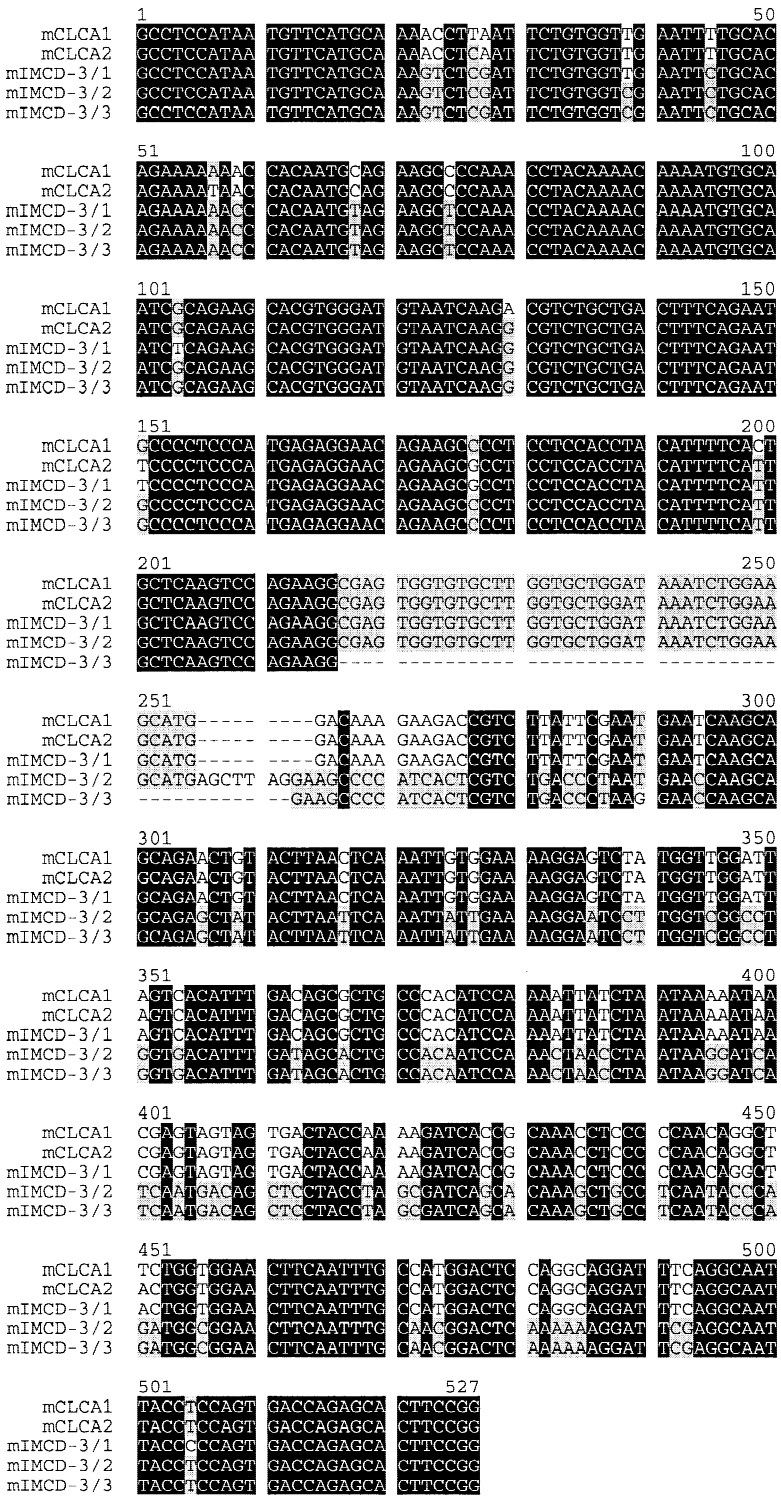


**Fig. 13.** Nucleotide sequence of the three IMCD-3 products. Alignment of the nucleotide sequences of the three RT-PCR cDNA products from mIMCD-3 cells (mIMCD-3/1, mIMCD-3/2 and mIMCD-3/3), with the known mouse homologues, mCLCA1 and 2. Note that the mIMCD-3/2 product contains an additional 9 bp insert at position 256, not seen in either mCLCA1 or 2. The shorter PCR product (mIMCD-3/3) contains a 46 bp deletion compared to mIMCD-3/2, but is otherwise identical. Dark highlighting indicates complete identity, and light highlighting indicates partial identity.

Translation and comparison of the predicted amino-acid sequence of the 3 transcripts from mIMCD-3 cells with mCLCA1 and mCLCA2 is shown in Fig. 14*A*. Multiple sequence alignment (Corpet, 1998) demonstrates that the mIMCD-3/1 product shares 165/173 amino acids in common with mCLCA1 (95.4% identity) and 167/173 amino acids in common with mCLCA2 (96.5% identity). The similarity of mIMCD-3/2 to mCLCA1 is less (139/176, 79.0% identity) and only 78.4% identity with mCLCA2 (138/176 amino acids)

suggesting that this transcript is likely to arise from a new gene for an additional mCLCA family member. Translation of the 481 bp product (IMCD-3/3) failed to reveal a complete open reading frame; rather there is frame shift arising from the deletion, that results in truncated protein product similar in nature to hCLCA3 (Gruber & Pauli, 1999). Protein motif analysis (PRINTS, Attwood et al., 1999) of the mIMCD-3/2 product, identified a transmembrane motif (TM), (RRVVCLVLDKSGSMSLGSPITR) with significant homology to the rhodopsin-like GPCR superfamily 7-element motifs (*see* Fig. 14*B*), which is absent in the other 2 transcripts. In conclusion our results provide evidence for multiple transcripts related to mCLCA in mIMCD-3 cells. Whether these transcripts arise from expression of multiple genes, or as a consequence of alternative splicing of a common gene, is presently unknown.

## Discussion

In this study we have demonstrated that the major $Cl^-$ conductance in mouse renal inner medullary collecting duct cells is regulated by $[Ca^{2+}]_i$. A novel finding from this study is that reduction or elevation of external calcium results in a corresponding decrease or increase in $[Ca^{2+}]_i$, which is accompanied by a parallel change in whole cell $Cl^-$ conductance. We show that the underlying mechanism for transducing alterations in external calcium into a change in $[Ca^{2+}]_i$ involves calcium influx across the plasma membrane, probably through calcium-selective channels and not via activation of polyvalent cation-sensing receptors. In addition, mobilization of calcium stores by extracellular nucleotides, or exposure to ionomycin, also leads to increases in $Cl^-$ currents, providing further evidence for calcium regulation of anion transport in these cells.

### Biophysical Properties of the $Ca^{2+}$-Activated $Cl^-$ Conductance

Calcium-activated $Cl^-$ channels are found in a variety of excitable and nonexcitable cells (Begenisich & Melvin, 1998). The kinetic properties of these $Cl^-$ currents measured with the patch clamp technique (whole cell and excised patches) varies with cell type. However, in the majority of secretory epithelia (Begenisich & Melvin, 1998) these currents display characteristic voltage-dependent kinetics. At intracellular calcium concentrations between 0.1 and 0.5 μM, currents usually display clear activation at depolarizing holding potentials and marked inactivation at hyperpolarizing potentials, with the resultant steady-state *I/V* plot being outwardly rectified. Evans and Marty (1986) demonstrated that this gating pattern was dependent on the prevailing intracellular calcium levels. As $[Ca^{2+}]_i$ increased (above μM levels in lacrimal acinar cells) the $Cl^-$ conductance not only increased in size but lost any clear voltage-dependence. Activation became essentially instantaneous, and little inactivation was observed resulting in an approximately linear, steady-state, *I/V* plot. We have observed a similar phenomenon in human pancreatic duct cells (Winpenny et al., 1998), and more recently showed identical kinetic changes in a single cell, after inducing slow ramps in $[Ca^{2+}]_i$, produced by exposing BAPTA-loaded mIMCD-K2 cells to ionomycin (Boese et al., 2000). Kumura and Hartzell (1999) have recently provided an explanation for this complex gating behavior after studying the kinetics of the intrinsic $Ca^{2+}$-activated $Cl^-$ channels of *Xenopus* oocytes plasma membrane. They concluded that the gating effects observed at low (0.1 μM) and high (0.6 μM) $[Ca^{2+}]_i$ could be explained by a single class of $Ca^{2+}$-activated $Cl^-$ channel, in which channel opening is $Ca^{2+}$-dependent but independent of voltage, whereas channel closing is voltage-sensitive.

The kinetic properties of the $Ca^{2+}$-activated $Cl^-$ conductance of mIMCD-3 cells is clearly different to the studies above. Basal current levels are remarkably large and comparable to those recorded from secretory epithelia only after agonist stimulation. The fact that the mIMCD-3 currents are present during 'slow' whole cell recording, where the endogenous calcium-buffering systems within the cell are left intact (Horn & Marty, 1988), indicates that they are likely to be active under quasi-physiological conditions, and therefore contribute to the resting $Cl^-$ permeability of these cells. We speculate that a basal calcium permeability in the plasma membrane of mIMCD-3 cells maintains CaCC activity, and it is this pathway which allows these cells to 'sense' external calcium concentration, and indirectly activate the channels. Nonetheless, there is no hint of any voltage-dependence in the current records at any of the conditions we have used. In addition, despite the lack of time and voltage-dependent relaxations, which could imply that the mIMCD-3 currents were maximally activated, a further increase in whole cell $Cl^-$ conductance was still observed upon ATP or ionomycin stimulation (with no change in kinetics). These differences in properties become even more pronounced when intracellular $Ca^{2+}$ is reduced, either by BAPTA-loading or incubation in low external calcium solutions. Despite a marked reduction in current magnitude the kinetic properties of the currents were unchanged (*see* Fig. 3), implying that neither calcium nor voltage modulates the gating of the channels.

Overall, our results imply that the kinetic properties of the $Ca^{2+}$-activated $Cl^-$ current of mIMCD-3 cells is different from those described for $Ca^{2+}$-dependent $Cl^-$ currents in many other secretory epithelia. However, the biophysical properties are very similar to those described

A

```
          1                                                  50
   mCLCA1 ASIMFMQNLN SVVEFCTEKN HNAEAPNLQN KMCNRRSTWD VIKTSADFQN
   mCLCA2 ASIMFMQNLN SVVEFCTENN HNAEAPNLQN KMCNRRSTWD VIKASADFQN
mIMCD-3/1 ASIMFMQSLD SVVEFCTEKT HNVEAPNLQN KMCNLRSTWD VIKASADFQN
mIMCD-3/2 ASIMFMQSLD SVVEFCTEKT HNVEAPNLQN KMCNRRSTWD VIKASAEFQN
mIMCD-3/3 ASIMFMQSLD SVVEFCTEKT HNVEAPNLQN KMCNRRSTWD VIKASADFQN

          51                                                 100
   mCLCA1 APPMRGTEAP PPPTFSLLKS RRRVVCLVLD KSGSMDKED- --RLIRMNQA
   mCLCA2 SPPMRGTEAP PPPTFSLLKS RRRVVCLVLD KSGSMDKED- --RLIRMNQA
mIMCD-3/1 SPPMRGTEAP PPPTFSLLKS RRRVVCLVLD KSGSMDKED- --RLIRMNQA
mIMCD-3/2 APPMRGTEAP PPPTFSLLKS RRRVVCLVLD KSGSMSLGSP ITRLTLMNQA
mIMCD-3/3 APPMRGTEAP PPPTFSLLKS RREAPSLV

          101                                                150
   mCLCA1 AELYLTQIVE KESMVGLVTF DSAAHIQNYL IKITSSSDYQ KITANLPQQA
   mCLCA2 AELYLTQIVE KESMVGLVTF DSAAHIQNYL IKITSSSDYQ KITANLPQQA
mIMCD-3/1 AELYLTQIVE KESMVGLVTF DSAAHIQNYL IKITSSSDYQ KITANLPQQA
mIMCD-3/1 AELYLIQIIE KESLVGLVTF DSTATIQTNL IRIINDSSYL AISTKLPQYP
mIMCD-3/1

          151                  176
   mCLCA1 SGGTSICHGL QAGFQAITSS DQSTSG
   mCLCA2 TGGTSICHGL QAGFQAITSS DQSTSG
mIMCD-3/1 TGGTSICHGL QAGFQAITPS DQSTSG
mIMCD-3/2 DGGTSICNGL KKGFEAITSS DQSTSG
mIMCD-3/3
```

B

```
mIMCD-3/1 ASIMFMQSLDSVVEFCTEKTHNVEAPNLQNKMCNLRSTWDVIKASADFQNSPPMRGTEAPPPPT
mIMCD-3/2 ASIMFMQSLDSVVEFCTEKTHNVEAPNLQNKMCNRRSTWDVIKASAEFQNAPPMRGTEAPPPPT
mIMCD-3/3 ASIMFMQSLDSVVEFCTEKTHNVEAPNLQNKMCNRRSTWDVIKASADFQNAPPMRGTEAPPPPT


mIMCD-3/1 FSLLKSRRRVVCLVLDKSGSMDKED---RLIRMNQAAELYLTQIVEKESMVGLVTFDSAAHIQN
mIMCD-3/2 FSLLKSRRRVVCLVLDKSGSMSLGSPITRLTLMNQAAELYLIQIIEKESLVGLVTFDSTATIQT
mIMCD-3/3 FSLLKSRREAPSLV


mIMCD-3/1 YLIKITSSSDYQKITANLPQQATGGTSICHGLQAGFQAITPSDQSTSG
mIMCD-3/2 NLIRIINDSSYLAISTKLPQYPDGGTSICNGLKKGFEAITSSDQSTSG
mIMCD-3/3
```

RRVVCLVLDKSGSMSLGSPITR = Rhodopsin-like GPCR motif

TEK, SRR and STK = putative protein kinase C sites
RRS = putative protein kinase A site

**Fig. 14.** Predicted amino-acid sequence of the three mIMCD-3 CLCA products. (*A*) The predicted amino acid sequences of the three mCLCA sequences are displayed together with the known sequences for mouse CLCA1 and 2. (*B*) The amino acid sequences of the three mIMCD-3 products only with the rhodopsin-like GPCR transmembrane domain motif highlighted for mIMCD3/2. Potential PKC and PKA phosphorylation sites indicated. Other details as in Fig. 13.

for mCLCA1 functionally expressed in HEK293 cells (Gandhi et al., 1998) and mCaCC heterologously expressed in *Xenopus* oocytes (Romio et al., 1999). In HEK293 cells, calcium-dependent currents were activated either by exposure to ionomycin or by inclusion of 2 mM $Ca^{2+}$ in the pipette during 'fast' whole cell patch-clamp recording. These $Ca^{2+}$-activated $Cl^-$ currents were outwardly rectifying, and time-independent. In *Xenopus* oocytes, in the absence of ionophore, mCaCC expression was associated with elevation of an outwardly rectifying, time-independent $Cl^-$ current. Taken together, these data show strong similarities to both the $Ca^{2+}$-dependent basal currents and the currents activated by ATP and ionomycin noted here for mIMCD-3 cells. However, the $Cl^-$ current present in mIMCD-3 cells shows two important differences to mCLCA1 expressed in HEK293 cells. First, current density measured at 80 mV is approximately 20-fold greater in the kidney cells

and secondly, the currents are active under resting conditions. These results suggest that the mIMCD-3 cells express a higher density of channels than the transfected cells and/or that the IMCD channels are more sensitive to calcium. It has been reported that the calcium-sensitivity of CACC from bovine tracheal cells is altered in a complex way by $Ca^{2+}$/calmodulin-dependent protein kinase II (CaMK II) phosphorylation, as well as by inositol 3,4,5,6-tetrakisphosphate ($IP_4$) levels (Ismailov et al., 1996). Mouse and human CLCA1 contain several potential phosphorylation sites for both CaMK II and protein kinase C (Gruber et al., 1998*a*), and a recent paper showed that the full length as well as a truncated form of bCLCA1 was stimulated by PKC activation (Ji et al., 1998). It is therefore possible that the high basal level of channel activity that we observe in mIMCD-3 cells is due to endogenous phosphorylation by these calcium-dependent kinases. Figure 14*B* shows that the potential phosphorylation sites present in the mCLCA1 sequence are also conserved in our second novel transcript. In addition, the fact that changes in whole cell conductance take many minutes following bath changes in calcium concentration, and that increase in $[Ca^{2+}]_i$ after ATP stimulation occurs far more rapidly than the subsequent change in current, argues for multiple regulatory steps being involved in regulating CACC in mIMCD-3 cells. We speculate that this involves direct channel phosphorylation, but it could also involve insertion and retrieval of channels from the plasma membrane, due to the time course involved.

### Molecular Identity of mIMCD-3 Chloride Currents

Using homology cloning Gandhi et al. (1998) identified a mouse homologue (mCLCA1) of the bovine tracheal $Ca^{2+}$-activated $Cl^-$ conductance (Cunningham et al., 1995) from a lung cDNA library. mCLCA1 is a member of a family of related mouse proteins since a new gene, mCLCA2, present in mammary gland has been described (Lee et al., 1999). Each family member appears to possess a distinct tissue expression pattern in mouse or human tissues (Angel et al., 1999; Gruber et al., 1998*b*, 1999). mCLCA1 is expressed in heart, lung, liver and kidney by Northern analysis (Gandhi et al., 1998). Tissue distribution of mCLCA1 was further investigated by Gruber et al. (1998*b*) using in situ hybridization, RT-PCR and Northern blotting. mCLCA1 was strongly expressed in mouse secretory tissue such as mammary gland, respiratory, and intestinal epithelia but also in other epithelial tissue including kidney, uterus and epididymis. However, a separate analysis of mCLCA1 distribution showed expression restricted to skin and kidney (Romio et al., 1999), a result that hasn't been explained. We have already reported identification of an RT-PCR product with strong homology to mCLCA1 from mIMCD-K2 cell mRNA (Boese et al., 2000). Our present data show that in another IMCD-derived cell-line, mIMCD-3, expression of an RT-PCR product related to mCLCA1/2 occurs, together with 2 additional transcripts that show significantly less identity to either mCLCA1 or the mammary form, mCLCA2. Our protein motif analysis of the mIMCD-3/2 product identified a transmembrane motif (RRVVCLVLDKSGSMSLGSPITR) with significant homology to the rhodopsin-like GPCR superfamily 7-element motifs (*see* Fig. 14*B*). This motif is not found in either mCLCA1 or mCLCA2, which suggests a different membrane topology to that proposed for mCLCA1 or hCLCA2, and therefore possibly a different function. However, without a complete nucleotide sequence for this second transcript, we can only speculate on its functional role. The third transcript identified in the present study is likely to represent a mouse homologue of the truncated 37 kD secreted protein (hCLCA3) identified by Gruber and Pauli (1999). The mouse protein is truncated at position 29 of the mIMCD-3/3 PCR product indicated in Fig. 14*B.* The function of this secreted protein is unknown but Gruber and Pauli (1999) suggest that it may function in signal transduction or competitive adhesion.

The presence of novel CLCA transcripts, although preliminary, suggests that mIMCD-3 cells may express multiple calcium-dependent channels. However, our pharmacological evidence did not provide any clear-cut evidence for this. Overall, DIDS, niflumic acid, glybenclamide and NPPB were equally effective as inhibitors of the basal and stimulated $Cl^-$ current. Only DTT provided any evidence for differences between the basal and agonist-stimulated currents, where it was found to only inhibit the basal $Cl^-$ currents in an irreversible way. This effect of DTT on basal currents is consistent with a reduction of disulfide bonds and the formation of free sulfhydryl groups on the channel protein. From sequence data it is known that CLCA proteins contain a cluster of cysteine residues within the large amino-terminal end of the protein (Gruber et al., 1998*a*, 1999), and these residues are likely to be the target of DTT in this case. When the basal current was increased by ATP or ionomycin, DTT exposure then either caused a further stimulation (ATP) or had no net inhibitory effect (ionomycin), and this occurred in a reversible manner, suggesting cysteine residues were not involved. This distinct pharmacological profile suggests that the same channel does not underlie the basal and agonist-stimulated currents. An alternative suggestion is that in the presence of increased levels of $Ca^{2+}$, the pharmacological properties of the channel are dramatically changed. The fact that the cells did not respond to ATP with an increase in conductance, but could still mobilize intracellular calcium, if they were first exposed to DTT,

is more consistent with the latter hypothesis. Overall, the pronounced effects of DTT on current size, and the dependency of the block on intracellular calcium, supports an important functional role for cysteine residues. DTT may thus prove to be a useful probe when investigating the properties of heterologously expressed $Ca^{2+}$-activated $Cl^-$ channels.

### Physiological Role of the $Ca^{2+}$-Activated $Cl^-$ Conductance in IMCD

$Ca^{2+}$-activated $Cl^-$ channels play a central role in linking secretory stimuli directly to transepithelial anion flow across the apical membrane (Begenisich & Melvin, 1998). Their importance to secretory epithelia is highlighted by the studies on CF knockout mice, which retain normal electrolyte and fluid secretion in the majority of tissues despite the absence of CFTR (Clark et al., 1994). The present data clearly show that ATP activates the $Cl^-$ conductance via a change in intracellular $Ca^{2+}$. Studies of reconstituted IMCD epithelial monolayers mounted in Ussing chambers, have also found that $Ca^{2+}$-mobilizing stimuli such as bradykinin or ATP stimulate transepithelial anion secretion (Boese et al., 2000; Kose, Simmons & Brown, 1997; McCoy et al., 1999) which is consistent with the $Cl^-$ conductance described in this report being present at the apical plasma membrane. Since a number of diverse stimuli are capable of raising intracellular $Ca^{2+}$ in IMCD cells (Zeidel, 1993), and since changes in extracellular calcium concentration can occur in the IMCD depending on physiological status, it is likely that the $Ca^{2+}$-activated $Cl^-$ conductance we have identified acts as an important effector to regulate Cl transport in this segment.

This work was supported by a Research Studentship to GS from the National Kidney Research Fund (MAG/NLS) and by grants from the British Heart Foundation (NLS) and the Wellcome Trust (MAG/NLS).

## References

Altschul, S.F., Madden, T.L, Schaffer, A.A., Zhang, J.H., Zhang, Z., Millar, W., Lipman, D.J. 1997. Gapped BLAST and PSI-BLAST: a new generation of protein database search programs. *Nucleic Acids Res.* **25:**3389–3402

Angel, M., Vermat, T., Culouscou, J-M. 1999. Identification of three novel members of the calcium-dependent chloride channel (CaCC) family predominantly expressed in the digestive tract and trachea. *FEBS Lett.* **455:**295–301

Atia, F., Zeiske, W., Van Driessche, W. 1999. Secretory apical $Cl^-$ channels in A6 cells: possible control by $Ca^{2+}$ and cAMP. *Pfluegers Arch.* **438:**344–353

Attwood, T.K., Flower, D.R., Lewis, A.P., Mabey, J.E., Morgan, S.R., Scordis, P., Selley, J.N., Wright, W. 1999. PRINTS prepares for the new millenium. *Nucleic Acids Res.* **27:**220–225

Begenisich, T., Melvin, J.E. 1998. Regulation of chloride channels in secretory epithelia. *J. Membrane Biol.* **163:**77–85

Boese, S.H., Glanville, M., Aziz, O., Gray, M.A., Simmons, N.L. 2000. $Ca^{2+}$ and cAMP-activated $Cl^-$ conductances mediate $Cl^-$ secretion in a mouse renal inner medullary collecting duct cells. *J. Physiol.* **523.2:**325–338

Bruce, J.I.E., Yang, X., Freguson, C.J., Elliot, A.C., Steward, M.C., Case, R.M., Riccardi, D. 1999. Molecular and functional identification of a $Ca^{2+}$ (polyvalent cation)-sensing receptor in rat pancreas. *J. Biol. Chem.* **274:**20561–20568

Clarke, L.L., Grubb, B.R., Yankaskas, J.R., Cotton, C.U., McKenzie, A., Boucher, R.C. 1994. Relationship of a non-cystic fibrosis transmembrane conductance regulator-mediated chloride conductance to organ-level disease in CFTR (−/−) mice. *Proc. Natl. Acad. Sci. USA* **91:**479–483

Corpet, F. 1998. Multiple sequence alignment with hierarchical clustering. *Nucleic Acids Res.* **16:**10881–10890

Cuffe, J.E., Bielfeld-Akerman, A., Thomas, J., Leipziger, J., Korbmacher, C. 2000. ATP stimulates $Cl^-$ secretion and reduces amiloride-sensitive $Na^+$ absorption in M-1 mouse cortical collecting duct cells. *J. Physiol.* **524.1:**77–90

Cunningham, S.A., Awayda, M.S., Bubien, J.K., Ismailov, I.I., Arrate, M.P., Berdiev, B.K., Benos, D.J., Fuller, C.M. 1995. Cloning of an epithelial channel from bovine trachea. *J. Biol. Chem.* **270:**31016–31026

Ecelberger, C.A., Maeda, Y., Gibson, C.C., Knepper, M.A. 1994. Extracellular ATP increases intracellular calcium in rat terminal collecting duct via a nucleotide receptor. *Am. J. Physiol.* **267:**F998–F1006

Evans, M.G., Marty, A. 1986. Calcium-dependent chloride currents in isolated cells from rat lacrimal glands. *J. Physiol.* **378:**437–460

Gandhi, R., Elble, R.C., Gruber, A.D., Schreur, K.D., Ji, H.-L., Fuller, C.M., Pauli, B.U. 1998. Molecular and functional characterization of a calcium-sensitive chloride channel from mouse lung. *J. Biol. Chem.* **273:**32096–32101

Glanville, M., Stewart, G.S., Gray, M.A., Pearce, S., Simmons, N.L. 1999. Molecular characterization of $Cl^-$ channel mRNA expression in mouse inner medullary collecting duct cells (mIMCD-3). *J. Physiol.* **515.P:**167P

Gray, M.A., Pollard, C.E., Harris, A., Coleman, L., Greenwell, J.R., Argent, B.E. 1990. Anion selectivity and block of the small conductance chloride channel on pancreatic duct cells. *Am. J. Physiol.* **259:**C752–C761

Gray, M.A., Plant, S., Argent, B.E. 1993. cAMP-regulated whole cell chloride currents in pancreatic duct cells. *Am. J. Physiol.* **264:**C591–C602

Gray, M.A., Winpenny, J.P., Porteous, D.J., Dorin, J.R., Argent, B.E. 1994. CFTR and calcium-activated chloride currents in pancreatic duct cells of a transgenic CF mouse. *Am. J. Physiol.* **266:**C213–C221

Gruber, A.D., Elble, R.C., Ji, H.-L., Schreur, K.D., Fuller, C.M., Pauli, B.U. 1998*a*. Genomic cloning, molecular characterization, and functional analysis of human CLCA1, the first human member of the family of $Ca^{2+}$-activated $Cl^-$ channel proteins. *Genomics.* **54:**200–214

Gruber, A.D., Gandhi, R., Pauli, B.U. 1998*b*. The murine calcium-sensitive chloride channel (mCACC) is widely expressed in secretory epithelia and in other select tissues. *Histochemical Cell Biology.* **110:**43–49

Gruber, A.D., Pauli, B.U. 1999. Molecular cloning and biochemical characterization of a truncated, secreted member of the human family of $Ca^{2+}$-activated $Cl^-$ channels. *Biochim. Biophys. Acta* **1444:**418–423

Gruber, A.D., Schreur, K.D., Ji, H.-L., Fuller, C.M., Pauli, B.U. 1999. Molecular cloning and transmembrane structure of hCLCA2 from

human lung, trachea, and mammary gland. *Am. J. Physiol.* **276:**C1261–C1270

Grynkiewicz, G., Poenie, M., Tsein, R.Y. 1985. A new generation of $Ca^{2+}$ indicators with greatly improved fluorescence properties. *J. Biol. Chem.* **260:**3440–3450

Hojgaard, I., Tiselius, H-G. 1999. Crystallization in the nephron. *Urol Res.* **27:**397–403

Horn, R., Marty, A. 1988. Muscarinic activation of ionic currents measured by a new whole-cell recording method. *J. Gen. Physiol.* **92:**145–159

Husted, R.F., Volk, K.A., Sigmund, R.D., Stokes, J.B. 1995. Anion secretion by the inner medullary collecting duct. *J. Clin. Invest.* **95:**644–650

Ismailov, I.V., Fuller, C.M., Berdiev, B.K., Shlyonsky, V.G., Benos, D.J., Barrett, K.E. 1996. A biologic function for an "orphan" messenger: D-myo-inositol 3,4,5,6-tetrakisphosphate selectively blocks epithelial calcium-activated chloride channels. *Proc. Natl. Acad. Sci. USA* **93:**10505–10509

Jentsch, T.J., Friedrich, A.S., Yamada, H. 1999. The CLC chloride channel family. *Pfluegers Arch.* **437:**783–795

Ji, H.-L., DuVall, M.D., Patton, H.K., Satterfield, C.L., Fuller, C.M., Benos, D.J. 1998. Functional expression of a truncated $Ca^{2+}$-activated $Cl^-$ channel and activation by phorbol ester. *Am. J. Physiol.* **274:**C455–C464

Kent, G., Iles, R., Bear, C.E., Huan, L-J,. Griesenbach, U., McKerlie, C., Frndova, H., Ackerley, C., Gosselin, D., Radzioch, D., O'Brodovich, H., Tsui, L-C., Buchwald, M., Tanswell, A.K. 1997. Lung disease in mice with cystic fibrosis. *J. Clin. Invest.* **100:**3060–3069

Kizer, N.L., Lewis, B., Stanton, B.A. 1995*a*. Electrogenic sodium absorption and chloride secretion by an inner medullary collecting duct cell line (mIMCD-K2). *Am. J. Physiol.* **268:**F347–355

Kizer, N.L., Vandorpe, D., Lewis, B., Bunting, B., Russell, J., Stanton, B.A. 1995*b*. Vasopressin and cAMP stimulate electrogenic chloride secretion in an IMCD cell line. *Am. J. Physiol.* **268:**F854–F861

Korbmacher, C., Volk, T., Segal, A.S., Boulpaep, E.L., Fromter, E. 1995. A calcium-activated and nucleotide-sensitive nonselective cation channel in M-1 mouse cortical collecting duct cells. *J. Membrane Biol.* **146:**29–45

Kose, H., Simmons, N.L., Brown, C.D.A. 1997. Bradykinin stimulates chloride secretion in an inner medullary collecting duct cell line (mIMCD-3). *J. Physiol.* **504:**P140

Kuruma, A., Hartzell, H.C. 1999. Bimodal control of a $Ca^{2+}$-activated $Cl^-$ channel by different $Ca^{2+}$ signals. *J. Gen. Physiol.* **115:**59–80

Lee, D., Ha, S., Kho, Y., Kim, J., Cho, K., Baik, M., Choi, Y. 1999. Induction of mouse $Ca^{2+}$-sensitive chloride channel 2 gene during involution of mammary gland. *Biochem. Biophys. Res. Comm.* **264:**933–937

Letz, B., Korbmacher, C. 1997. cAMP stimulates CFTR-like $Cl^-$ channels and inhibits amiloride-sensitive $Na^+$ channels in mouse CCD cells. *Am. J. Physiol.* **272:**C657–C666

Lloyd, S.E., Pearce, S.H.S., Fisher, S.E., Steinmeyer, K., Schwappach, B., Scheinman, S.J., Harding, B., Bolino, A., Devoto, M., Goodyer, P., Rigden, S.P.A., Wrong, O., Jentsch, T.J., Craig, I.W., Thakker, R.V. 1996. A common molecular basis for three inherited kidney stone diseases. *Nature* **379:**445–449

McCoy, D.E., Taylor, A.L., Kudlow, B.A., Karlson, K., Slattery, M.J., Schwiebert, L.M., Schwiebert, E.M., Stanton, B.A. 1999. Nucleotides regulate NaCl transport in mIMCD-K2 cells via P2X and P2Y purinergic receptors. *Am. J. Physiol.* **277:**F552–F559

Morales, M.M., Carrol, T.P., Morita, T., Schwiebert, E.M., Devuyst, O., Wilson, P.D., Lopes, A.G., Stanton, B.A., Dietz, H.C., Cutting, G.R., Guggino, W.B. 1996. Both the wild type and a functional isoform of CFTR are expressed in kidney. *Am. J. Physiol.* **270:**F1038–F1048

Rauchman, M.I., Nigam, S.K., Delpire, E., Gullans, S.R. 1993. An osmotically tolerant inner medullary collecting duct cell line from an SV40 transgenic mouse. *Am. J. Physiol.* **265:**F416–F424

Romio, L., Musante, L., Cinti, R., Seri, M., Moran, O., Zegarra-Moran, O., Galietta, L.J.V. 1999. Characterization of a murine gene homologous to the bovine CaCC chloride channel. *Gene* 228:181–188

Rubera, I., Tauc, M., Verheecke-Mauze, C., Bidet, M., Poujeol, C., Touret, N., Cuiller, B., Poujeol, P. 1999. Regulation of cAMP-dependent chloride channels in DC1 immortalized rabbit distal tubule cells in culture. *Am. J. Physiol.* **276:**F104–F121

Sands, J.M., Naruse, M., Baum, M., Jo, I., Hebert, S.C., Brown, E.M., Harris, H.W. 1997. Apical extracellular calcium/polyvalent cation-sensing receptor regulates vasopressin-elicited water permeability in rat kidney inner medullary collecting duct. *J. Clin. Invest.* **99:**1399–1405

Shindo, M., Simmons, N.L., Gray, M.A. 1996. Characterization of whole cell chloride conductances in a mouse inner medullary collecting duct cell line mIMCD-3. *J. Membrane Biol.* **149:**21–31

Simmons, N.L. 1993. Renal epithelial $Cl^-$ secretion. *Exper. Physiol.* **78:**117–137

Simon, D.B., Bindra, R.S., Mansfield, T.A., Nelson-Williams, C., Mendonca, E., Stone, R., Schurman, S., Nayir, A., Alpay, H., Bakkaloglu, A., Rodriguez-Soriano, J., Morales, J.M., Sanjad, S.A., Taylor, C.M., Pilz, D., Brem, A., Trachtman, H., Griswold, W., Richard, G.A., John, E., Lifton, R.P. 1997. Mutations in the chloride channel gene, CLCNKB, cause Bartter's syndrome type III. *Nat. Genet.* **17:**171–178

Stanton, B.A. 1989. Characterization of apical and basolateral membrane conductances of rat inner medullary collecting duct. *Am. J. Physiol.* **256:**F862–F868

Stewart, G.S., Aziz, O., Simmons, N.L., Gray, M.A. 1999. ATP stimulates a chloride conductance in mIMCD-3 cells by a $Ca^{2+}$-dependent mechanism. *J. Physiol.* **517.P:**14P

Vandorpe, D., Kizer, N., Ciampollilo, F., Moyer, B., Karlson, K., Guggino, W.G., Stanton, B.A. 1995. CFTR mediates electrogenic secretion in mouse inner medulla collecting duct (mIMCD-K2) cells. *Am. J. Physiol.* **269:**C683–C689

Winpenny, J.P., Verdon, B., McAlroy, H.L., Colledge, W.H., Ratcliff, R., Evans, M.J., Gray, M.A., Argent, B.E. 1995. Calcium-activated chloride conductance is not increased in pancreatic duct cells of CF mice. *Pfluegers Arch.* **430:**26–36

Winpenny, J.P., Harris, A., Hollingsworth, M.A., Argent, B.E., Gray, M.A. 1998. Calcium-activated chloride conductance in a pancreatic adenocarcinoma of ductal origin (HPAF) and in freshly isolated human pancreatic duct cells. *Pfluegers Arch.* **435:**796–803

Zeidel, M.L. 1993. Hormonal regulation of inner medullary collecting duct sodium transport. *Am. J. Physiol.* **265:**F159–F173